Electronic Supplementary Material (ESI) for Journal of Materials Chemistry A.

Electronic Supplementary Information

Design and Synthesis of a Covalent Organic Framework Bridging CdS Nanoparticles and Homogeneous Cobalt-Bipyridine Co-catalysts for a Highly Efficient Photocatalytic CO_2 Reduction

Khai H. Do, D. Praveen Kumar, A. Putta Rangappa, Jehee Lee, Sungin Yun, and Tae Kyu Kim*

Department of Chemistry, Yonsei University, Seoul 03722, Republic of Korea

*Corresponding Author: E-mail: tkkim@yonsei.ac.kr

Experimental Section

Synthesis of TpBD COF. TpBD was prepared by the identical method of synthesis of TpBpy using 621.81 mg of biphenyl-4, 4'-diamine (BD) (3.375 mmol) instead of 2, 2'-bipyridine 4, 4'-diamine (Bpy). A red solid precipitate was collected after the mixture was cooled normally off to room temperature. The precipitate was washed with a copious amount of distilled water and ethanol and then dried at 80 ^{o}C for 12 hours (Yield: ~ 750 mg, 77%).

350 mg of the raw material was cleaned using Soxhlet method with THF for 2 days and acetone for 2 days. Finally, the final product was washed with DMAc and DCM and then dried at 80 °C for 12 hours (Isolated yield ~ 192 mg, 55 %).

Synthesis of CdS/TpBD-20%. CdS/TpBD-20% was prepared by the identical method of synthesis of CdS/TpBpy using 57.78 mg of TpBD instead of TpBpy.

Synthesis of CdS/TpBpy-20%/Co. 50.00 mg of CdS/TpBpy-20% were treated with 8.0 mg of $CoCl_2.6H_2O$ in 15.0 mL of MeCN for 4 hours at room temperature. The solid was collected by centrifugation, washed with a copious amount of MeCN (8x7 ml), and dried at 80 °C for 12 hours.

Characterization methods. The CdS and Co concentrations in the photocatalysts were determined by an inductively coupled plasma optical emission spectrometer (OPTIMA 8300 ICP-OES). The Fourier transform infrared (FT-IR) spectra were obtained using a FT-IR spectrometer Vertex 70. A Bruker AVANCE II 400 MHz spectrometer was operated to collect the solid state ^{13}C NMR result of TpBpy. The X-ray diffraction (XRD) patterns of the powder samples were recorded on a Rigaku Ultima IV X-ray diffractometer using Cu Kα radiation as the X-ray source. The UV-VIS absorption measurements were performed using a V-770 UV-VIS/ NIR spectrophotometer. The compositions and chemical states of the as-synthesized samples were analyzed based on X-ray photoelectron spectroscopy using a Thermo Scientific Inc., U.K K-alpha system equipped with a monochromated Al Kα X-ray source (1486.6 eV) at a power of 36 W (12 kV/3 mA). Depth profile XPS studies were performed by etching the surface with a 1 keV Ar ion beam with a raster size of 2 mm x 2 mm. The Nitrogen adsorption and desorption measurements were carried out at 77 K using a Quantachrome Autosorb-iQ 2ST/MP. The CO_2 adsorption and desorption isotherms were obtained using a 3Flex Version 5.00 apparatus at 273.15 K. Transmission electron microscopy (TEM) images and EDS mappings were obtained by using

a JEOL JEM-F200 microscope equipped with EDS applying an accelerating voltage of 200 kV to characterize the microstructure properties. Surface morphology was evaluated using a field-emission scanning electron microscope (FESEM, JSM-7000F, JEOL). Focused ion beam SEM (FIB SEM) imaging was performed using a ZEISS Crossbeam 540 microscope. Aberration-corrected annular dark-field scanning transmission electron microscopy (AC-ADF-STEM) images and EDS mappings were collected by using a JEOL JEM-ARM200F NEOARM microscope equipped with EDS applying an accelerating voltage of 200 kV. The room temperature photoluminescence (PL) emission spectra were obtained on a Horiba spectrofluorometer (FluoroMax Plus). The time-resolved photoluminescence (TRPL) studies were conducted using a laser diode (Horiba DeltaDiode DD-375L) with a wavelength of 375 nm and the emission intensity was monitored at 520 nm.

Photoelectrochemical measurements. Photoelectrochemical experiments were conducted on a CHI 617B electrochemical workstation using a standard three-electrode system with a platinum wire counter electrode, and a silver/silver chloride (Ag/AgCl) reference electrode. A 0.5 M Na_2SO_4 aqueous solution served as the supporting electrolyte. A slurry containing 5.00 mg of an as-synthesized material, 450 μL ethanol, and 50 μL Nafion was spread onto the pretreated indium tin oxide (ITO) conductor glass substrate and dried under reduced pressure. A 150 W Xe lamp equipped with an AM 1.5G filter was used for irradiation at an intensity of 1 sun. Electrochemical impedance spectroscopy (EIS) was carried out at open-circuit potential with an AC voltage magnitude of 5 mV. The standard potentiostat equipped with an impedance spectra analyzer was run under the dark condition to record Mott−Schottky plots at a frequency of 0.2 and 1.0 kHz. The measured potentials versus Ag/AgCl were converted to the normal hydrogen electrode (NHE) scale by $E_{NHE} = E_{Ag/AgCl} + 0.197$.

Apparent quantum efficiency tests. The apparent quantum efficiency (AQE) was determined under similar experimental conditions of the CO_2 photoreduction, except the 150 W Xe irradiation source was fitted with different wavelength bandpass filters. A Model 15151 calibrated Si reference cell (ABET Technologies) was used to measure the output intensity. The apparent quantum efficiency (QE) was calculated by the following equation:

$$QE = \frac{number\ of\ reacted\ electrons}{number\ of\ incident\ photons} \times 100\% = \frac{(n_{CO} \times 2 + n_{H_2} \times 2) \times N_A}{number\ of\ incident\ photons} \times 100\%$$

Recycling tests. A larger amount of photocatalyst (4.00 mg) was used. After 3-hour illumination, the used catalyst was collected by centrifugation, washed with water (3x7 ml), and EtOH (2x7 ml), and then dried under reduced pressure at room temperature. Then, the operation was repeated as noted in CO_2 photoreduction experiments.

Supporting Figures

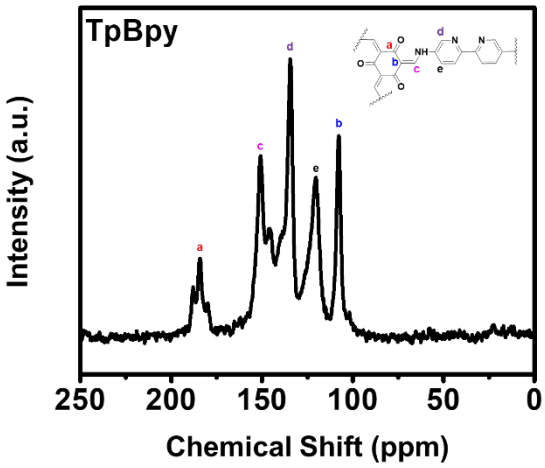

Figure S1 Solid-state ^{13}C NMR spectrum of TpBpy.

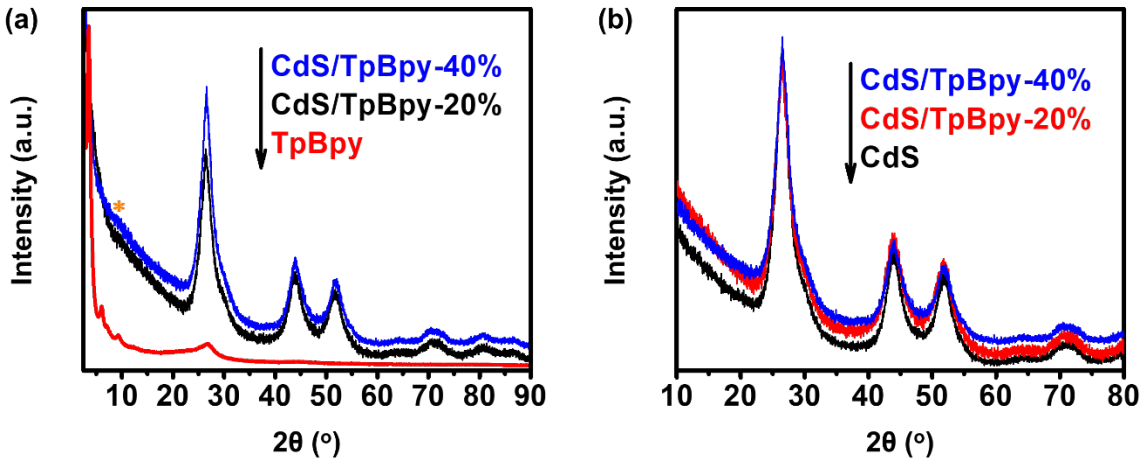

Figure S2 (a) Normalized XRD patterns of TpBpy and CdS/TpBpy composites in the range of 3–90° (* denotes the TpBpy singal). (b) Normalized XRD patterns of CdS and CdS/TpBpy composites in the range of 10–80° (to minimize the influences of background at low scattering angles and the amount of samples).

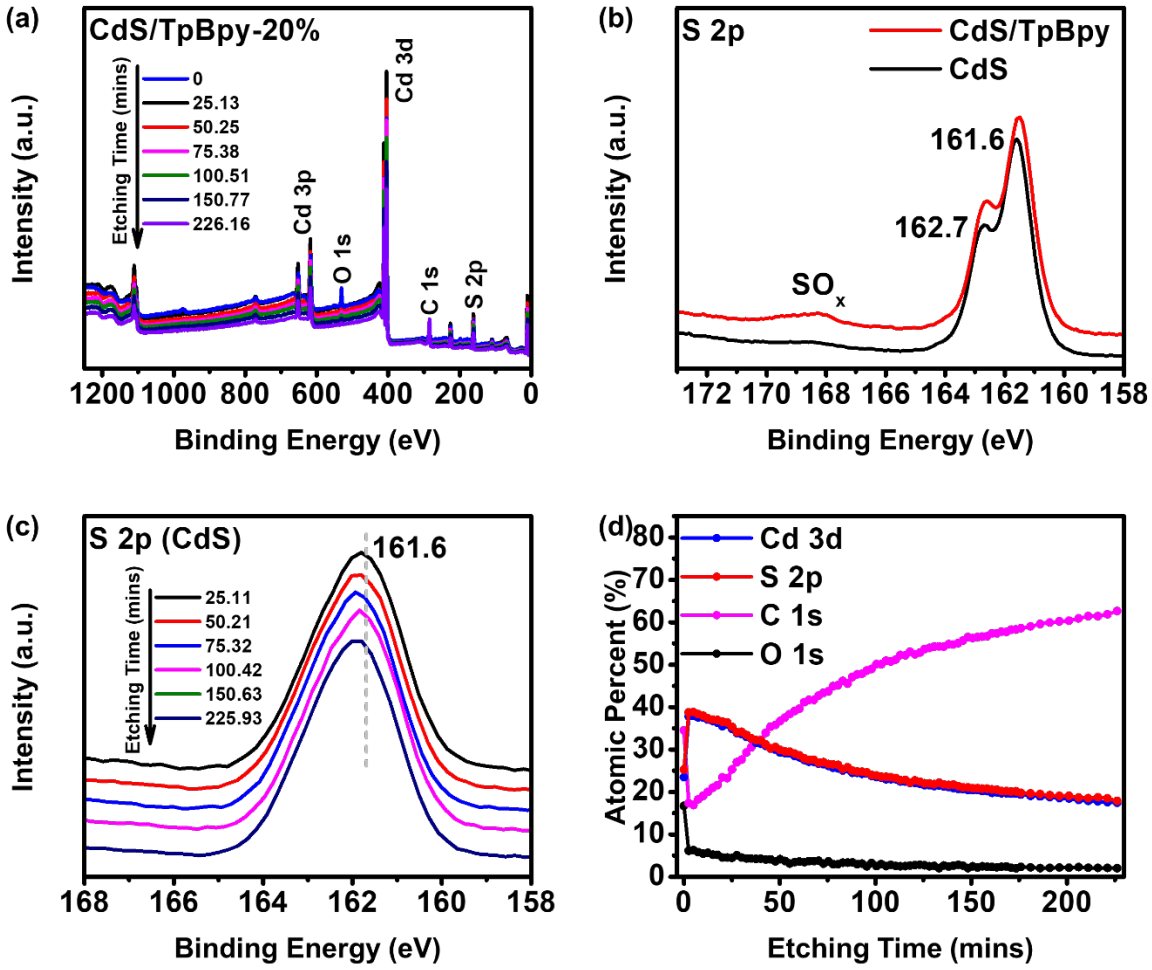

Figure S3 (a) XPS survey spectrum of the as-prepared composites. (b) S 2p high resolution XPS spectra at the surface of CdS/TpBpy and CdS. (c) S 2p high resolution XPS spectra of CdS at different etching times. (d) XPS atomic percentage of CdS/TpBpy-20%.

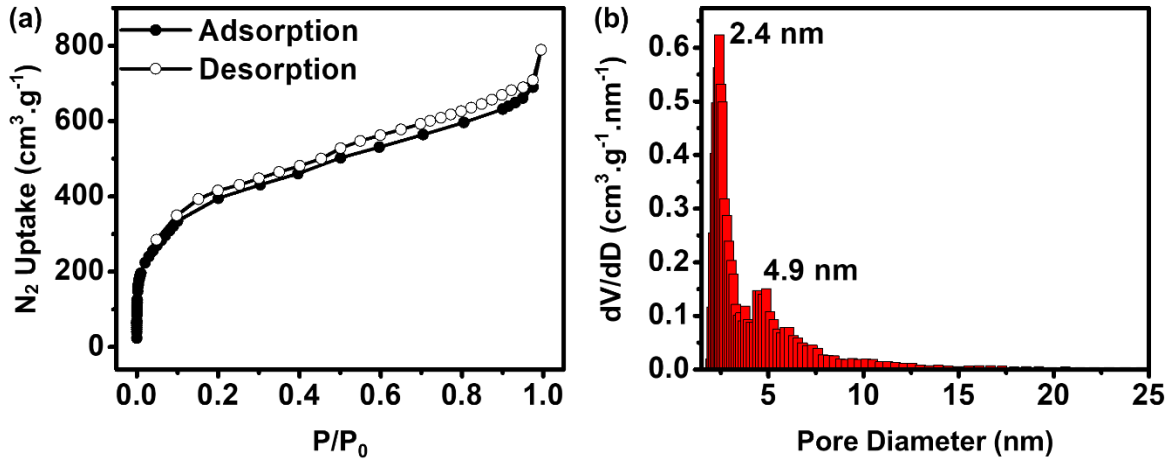

Figure S4 (a) N_2 adsorption–desorption isotherms and (b) pore size distribution of TpBpy. BET specific surface area and pore volume of TpBpy were calculated to be 1468.733 m^2g^{-1}, and 1.089 cm^3g^{-1}, respectively.

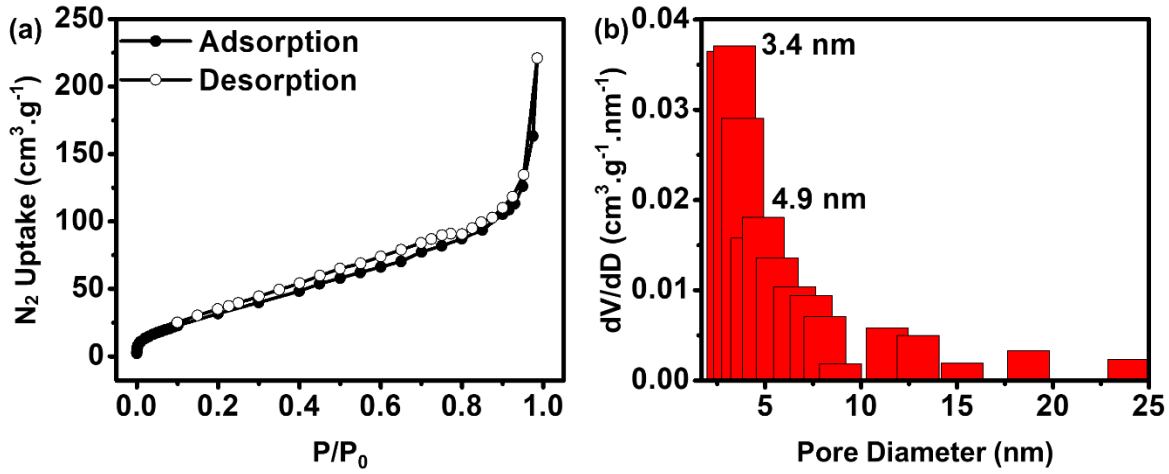

Figure S5 (a) N_2 adsorption–desorption isotherms and (b) pore size distribution of CdS/TpBpy-20%. BET specific surface area and pore volume of CdS/TpBpy-20% were calculated to be 136.384 m^2g^{-1}, and 0.318 cm^3g^{-1}, respectively.

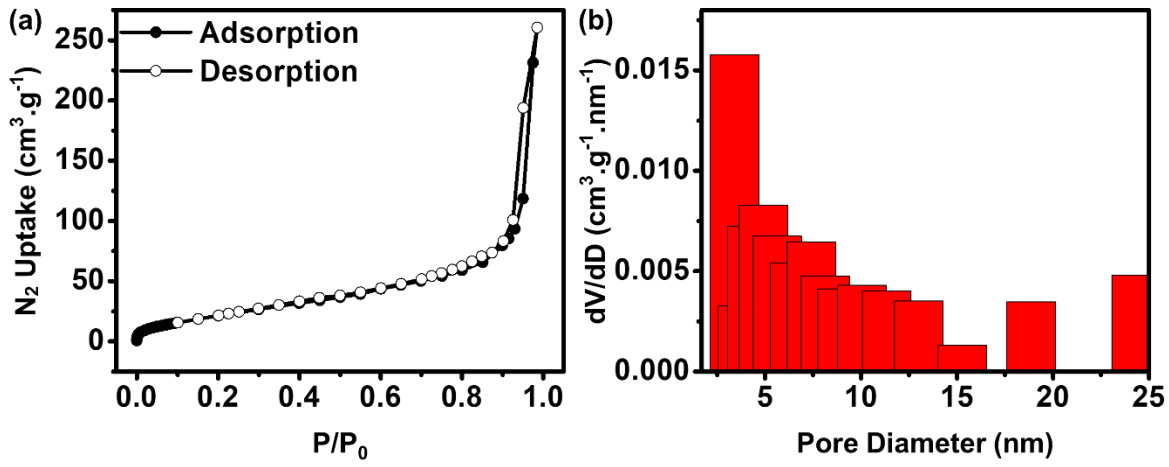

Figure S6 (a) N_2 adsorption–desorption isotherms and (b) pore size distribution of CdS. BET specific surface area and pore volume of CdS were calculated to be 89.698 m^2g^{-1}, and 0.389 cm^3g^{-1}, respectively.

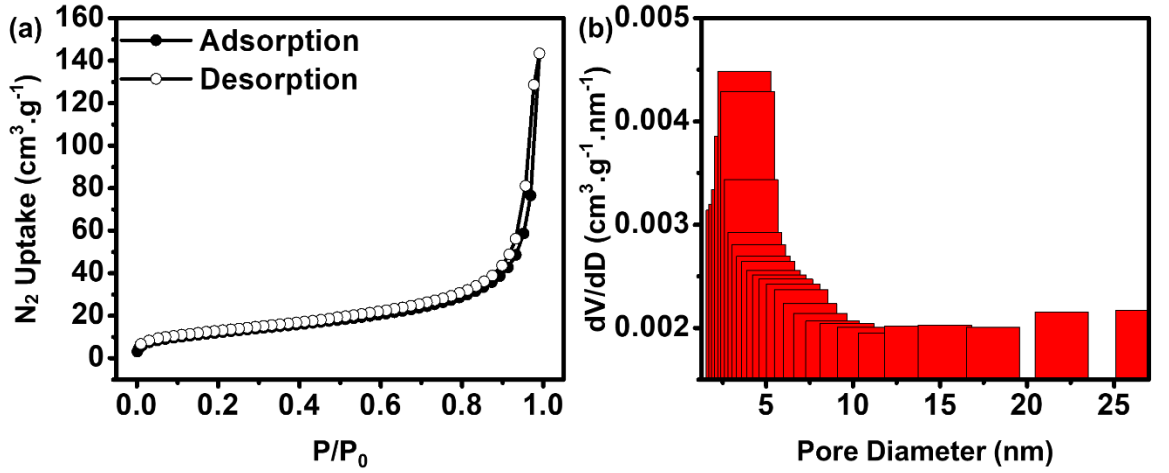

Figure S7 (a) N_2 adsorption–desorption isotherms and (b) pore size distribution of CdS/TpBpy-20%/Co. BET specific surface area and pore volume of CdS/TpBpy-20%/Co were calculated to be 44.524 m^2g^{-1}, 0.218 cm^3g^{-1} respectively.

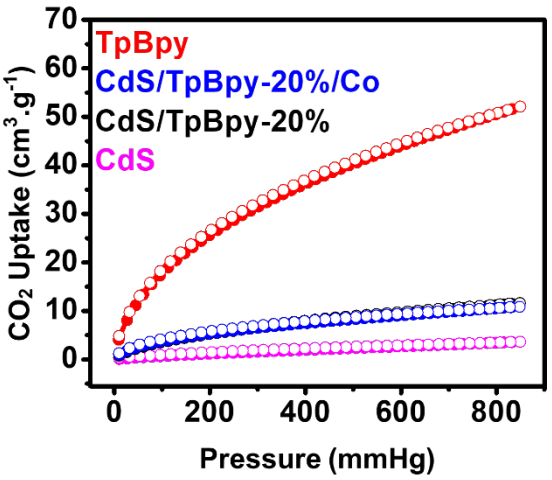

Figure S8 CO_2 adsorption–desorption isotherms of CdS, TpBpy, CdS/TpBpy-20%, and CdS/TpBpy-20%/Co.

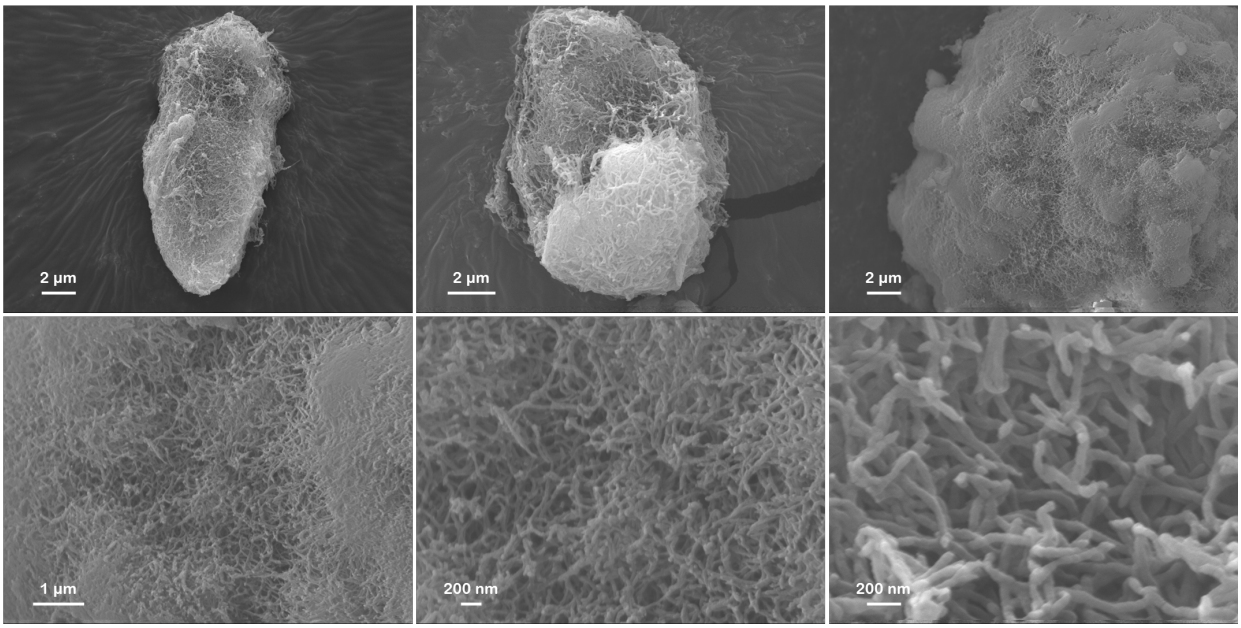

Figure S9 SEM images of TpBpy.

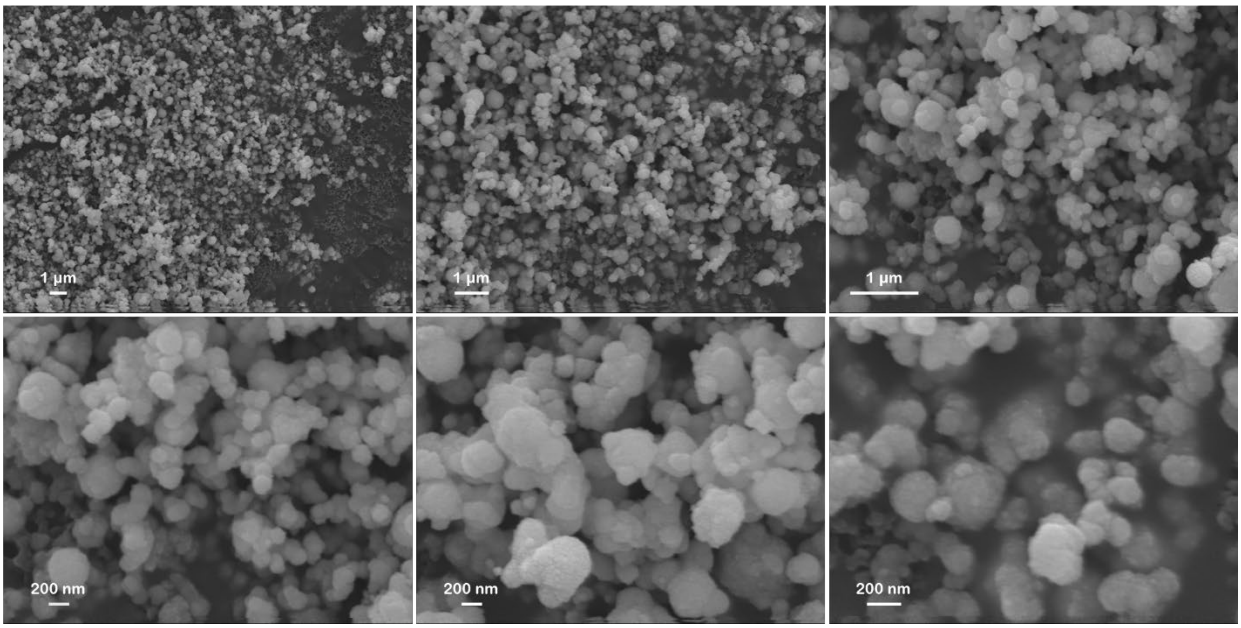

Figure S10 SEM images of CdS.

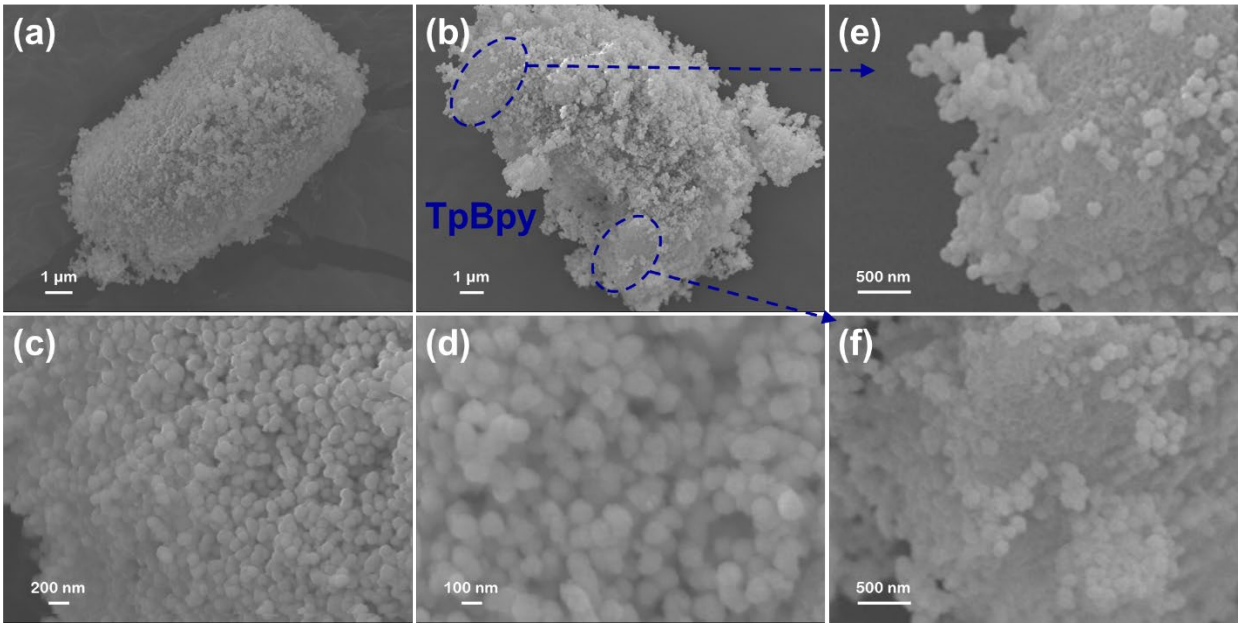

Figure S11 (a), (b), (c), and (d) SEM images of CdS/TpBpy. (e) and (f) Magnified views of (b) SEM image of CdS/TpBpy.

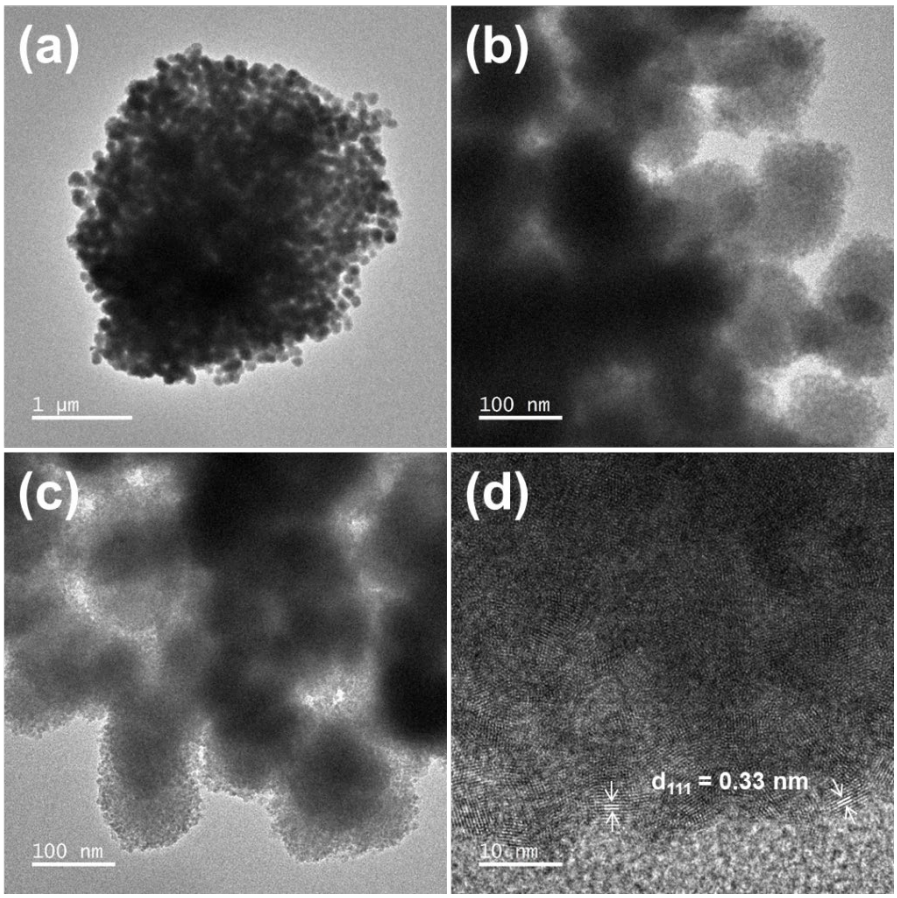

Figure S12 (a), (b), and (c) TEM images of CdS/TpBpy. (d) HRTEM image of CdS/TpBpy

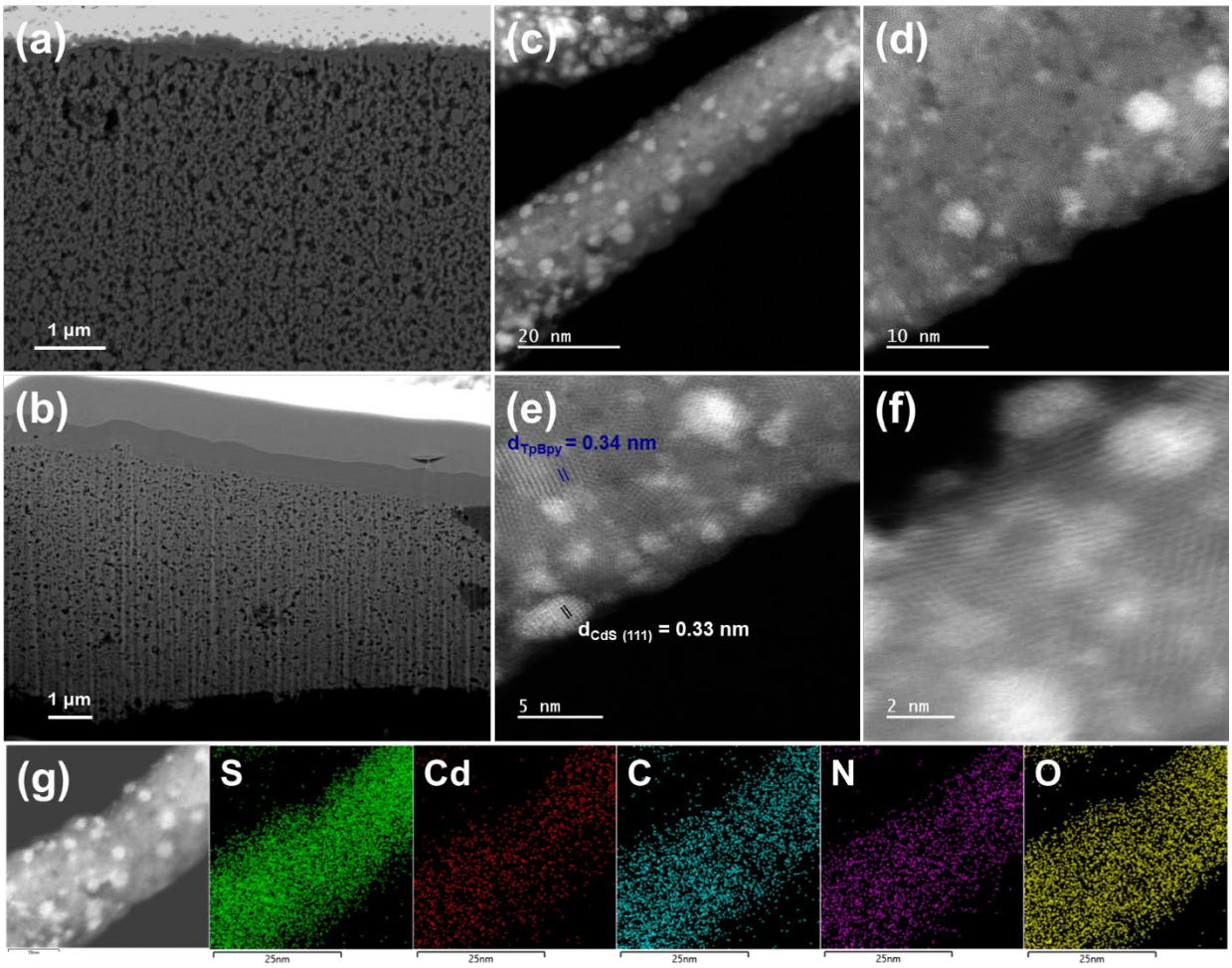

Figure S13 (a) and (b) FIB SEM images of CdS/TpBpy. (c), (d), (e), and (f) FIB AC-ADF-STEM images of CdS/TpBpy. (g) STEM EDX elemental mapping images of CdS/TpBpy.

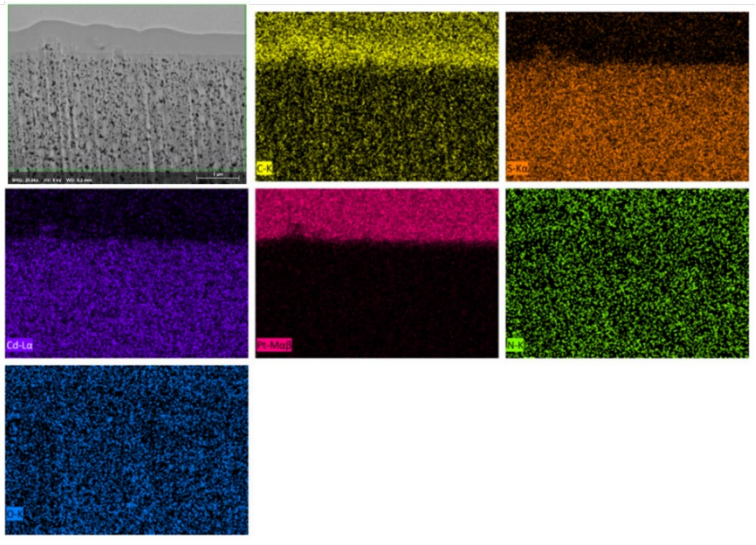

Figure S14 FIB SEM EDX elemental mapping images of CdS/TpBpy.

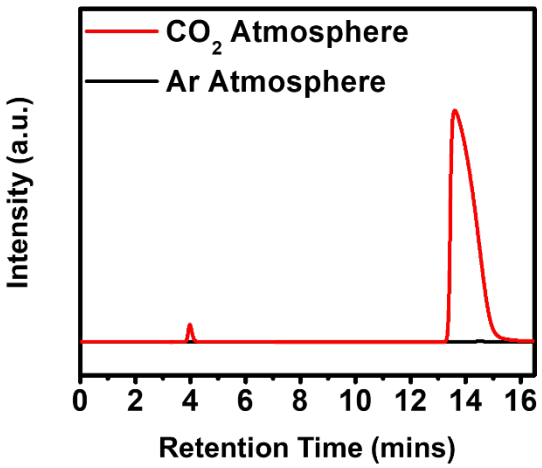

Figure S15 Gas chromatography (GC) results of the photocatalytic reductions under CO_2 and Ar environments. Retention times of CO and CO_2 are 4.0 and 13.7 mins, respectively.

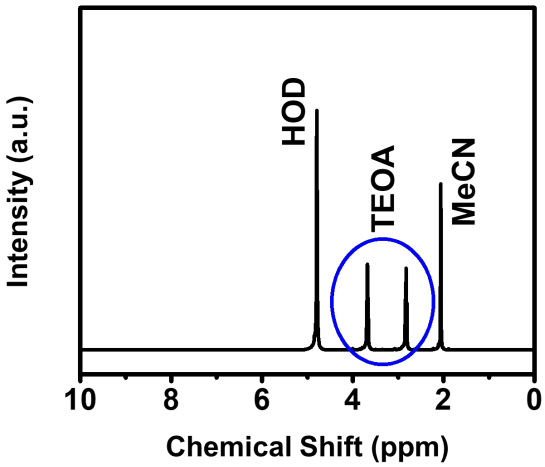

Figure S16 ^{1}H NMR spectrum of the liquid phase obtained from the reaction system after the CO_2 photoreduction reaction.

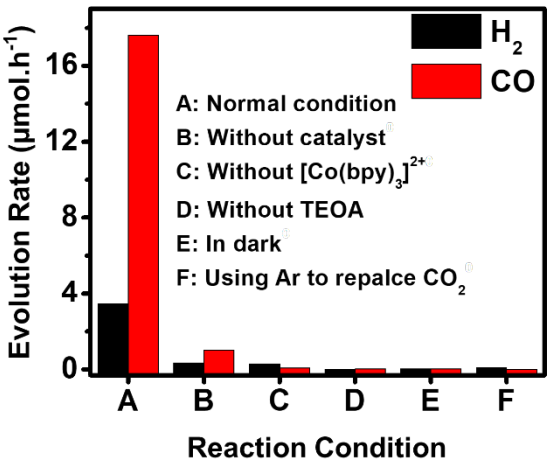

Figure S17 CO_2 photoreduction performances under various experimental conditions.

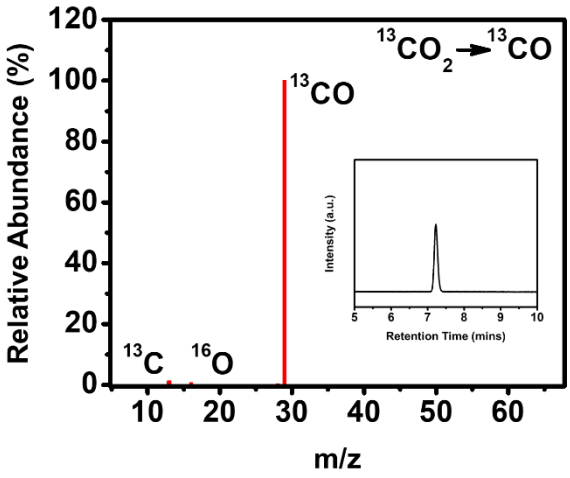

Figure S18 Mass spectrum of ^{13}CO generated from the $^{13}CO_2$-labeling experiment with the ^{13}CO peak (inset).

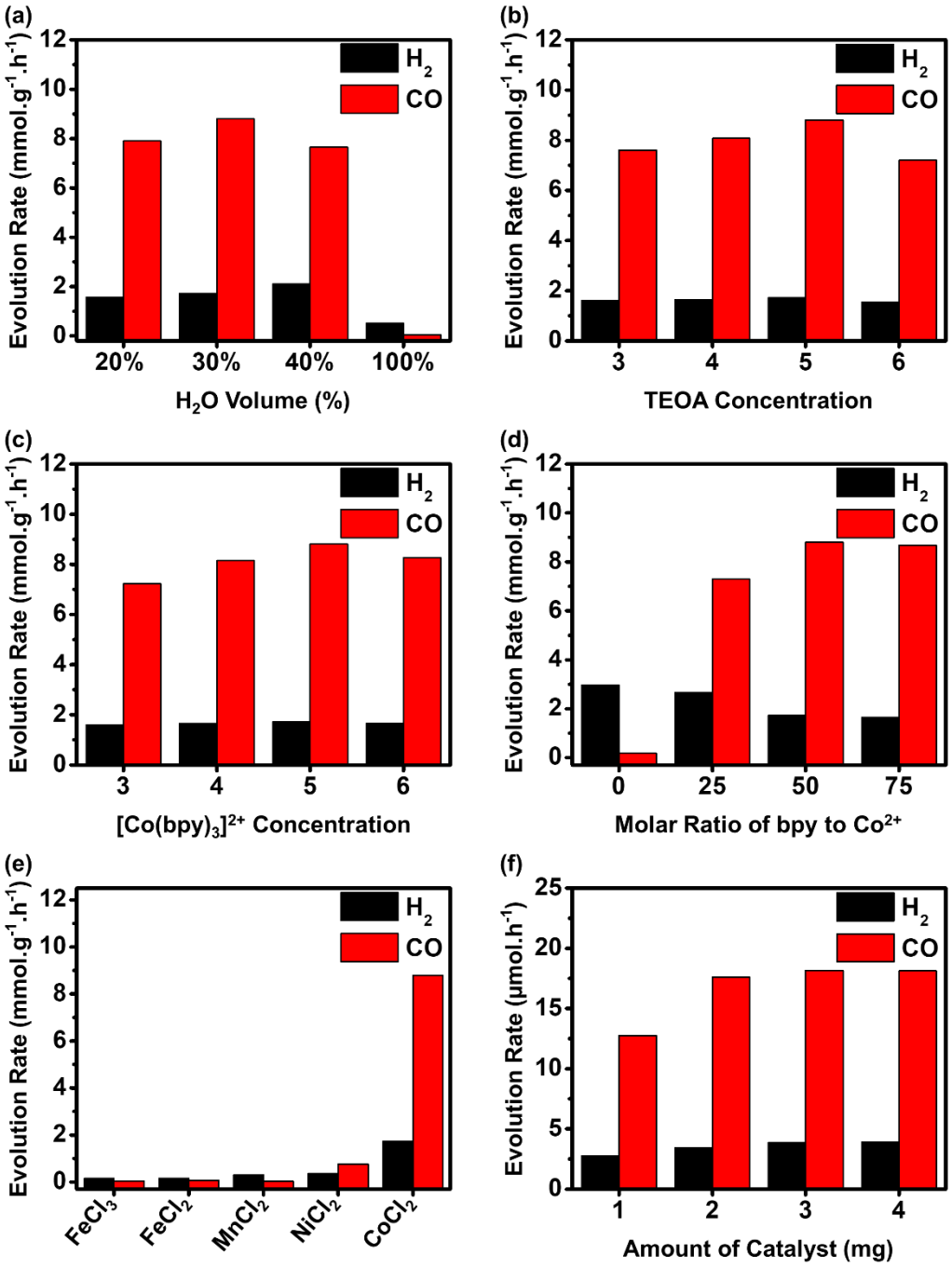

Figure S19 (a) Production of CO and H_2 as a function of water content in the 10.0 ml mixture solvent of H_2O/MeCN. Reaction condition: 2.00 mg of CdS/TpBpy-20%, 5.0 ml of TEOA, 5.00 μmol of $CoCl_2$, 250.0 μmol of bpy. (b) Influence of TEOA concentration on the photocatalytic CO_2 reduction performance. Reaction condition: 2.00 mg of CdS/TpBpy-20%, 5.00 μmol of $CoCl_2$, 250.0 μmol of bpy in the 15.0 ml solution. (c) Influence of $[Co(bpy)_3]^{2+}$ concentration (Co^{2+}/bpy = 1:50) on the photocatalytic performance of the optimized composite. (d) Influence of molar ratio of bpy to Co^{2+} (mole of Co^{2+} = 5.00 μmol) on the photocatalytic performance. (e) Influence of metal ions on the photocatalytic performance. (f) Influence of photocatalyst dosage on the photocatalytic CO_2 reduction performance.

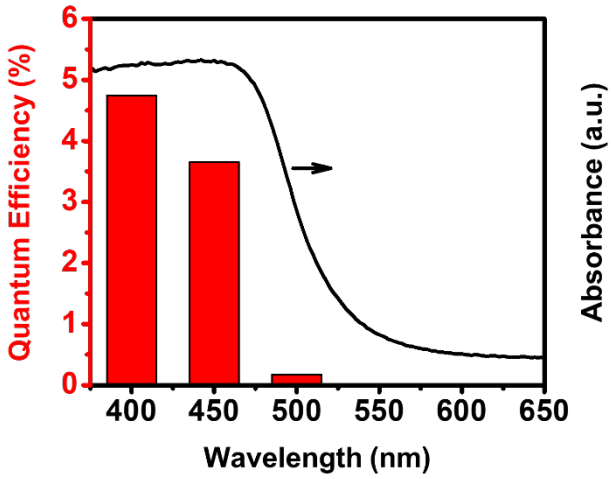

Figure S20 Quantum efficiency of the optimized composite.

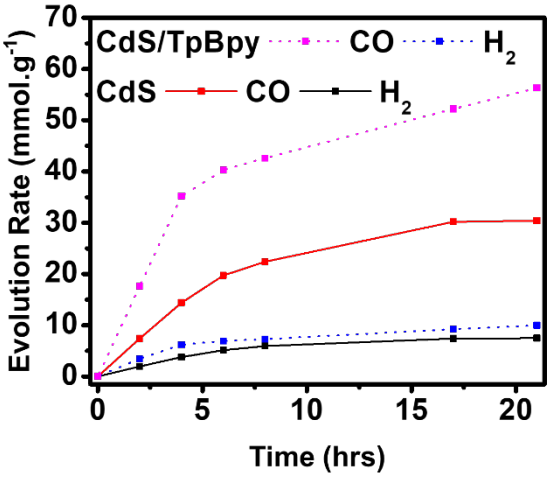

Figure S21 Time-yield plots of CO and H_2 over CdS/TpBpy and CdS.

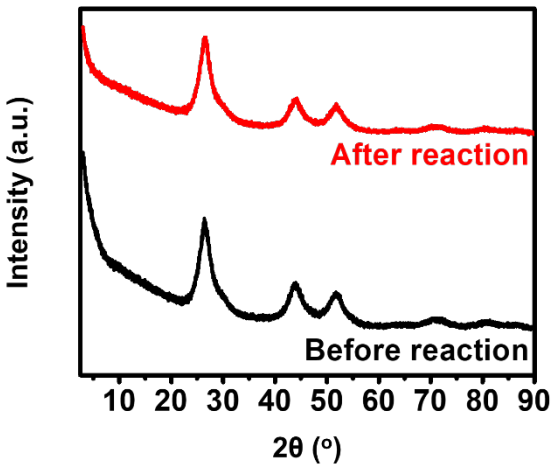

Figure S22 XRD patterns of fresh and used CdS/TpBpy after 6 cycles.

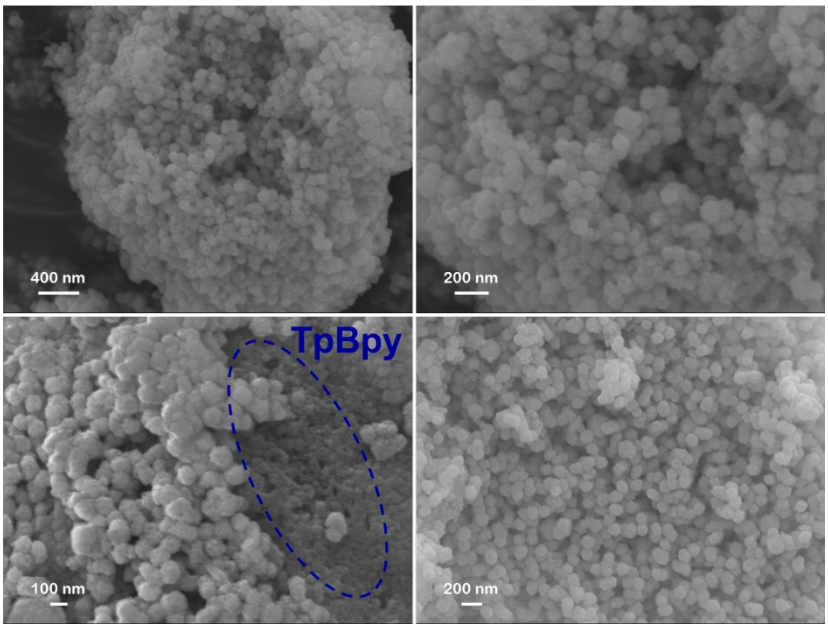

Figure S23 SEM images of CdS/TpBpy after recycling tests.

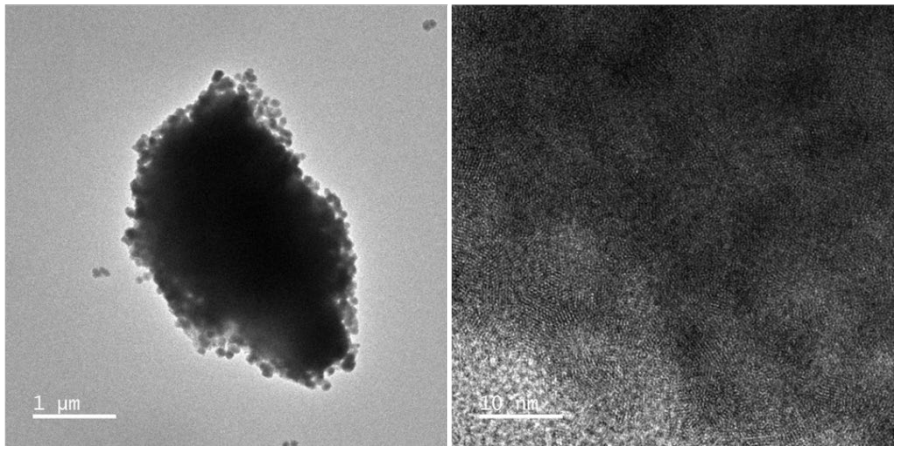

Figure S24 TEM images of CdS/TpBpy after recycling tests.

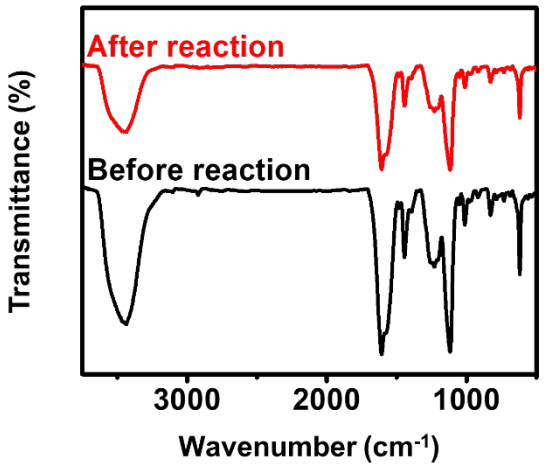

Figure S25 FT-IR spectra of fresh and used CdS/TpBpy.

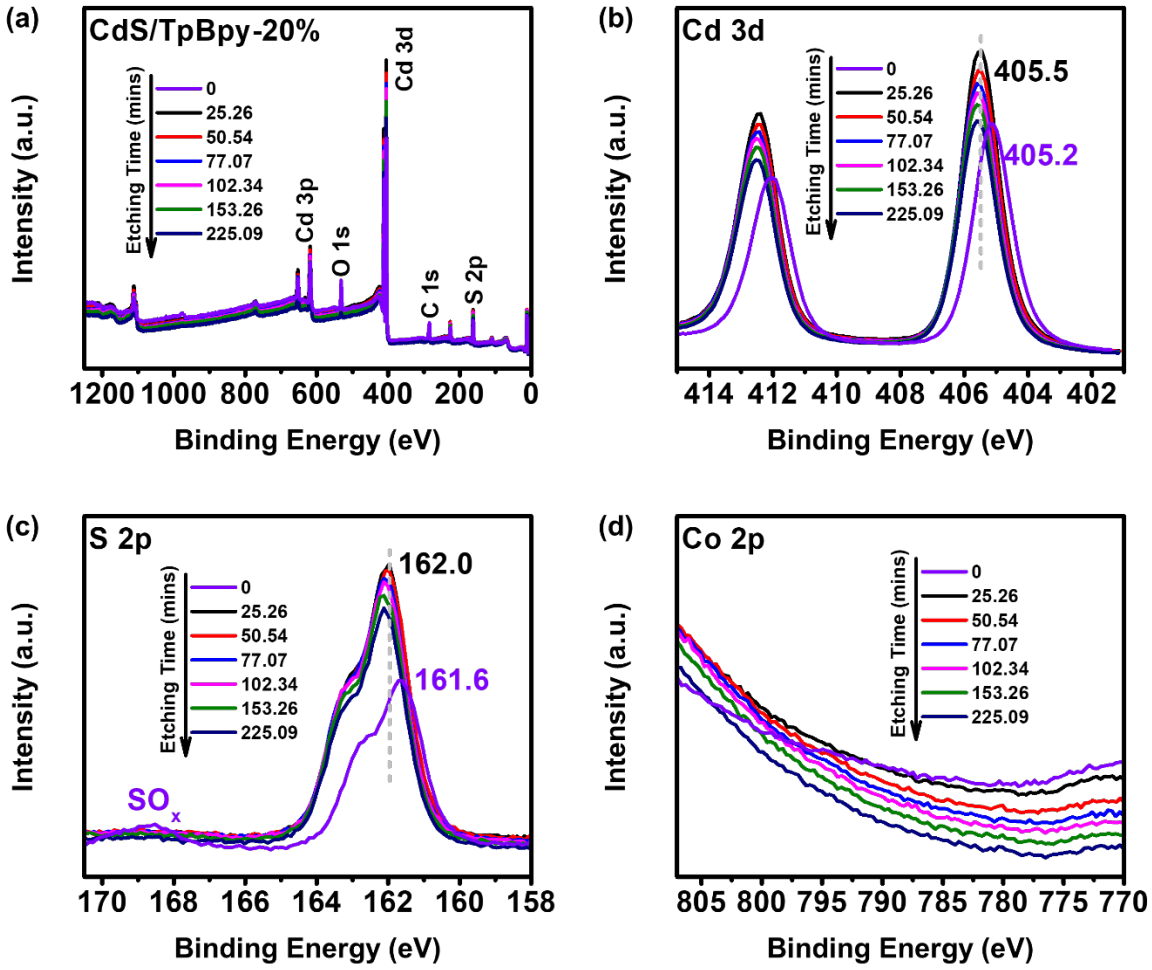

Figure S26 (a) XPS survey spectrum of used CdS/TpBpy. (b) Cd 3d, (c) S 2p, and (d) Co 2p high resolution XPS spectra of used CdS/TpBpy.

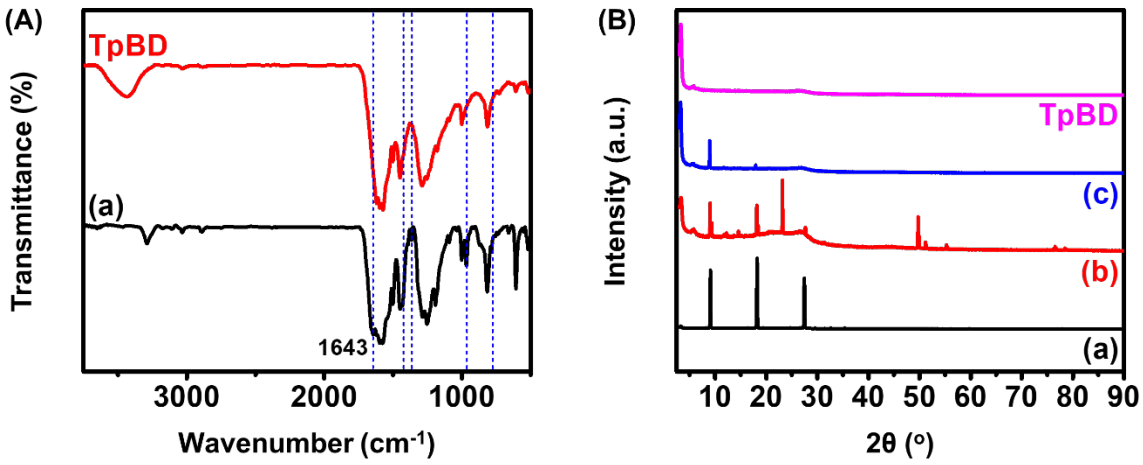

Figure S27 (A) FT-IR spectra of the raw material washed with (a) water and EtOH; and TpBD. (B) XRD patterns of the raw material washed with (a) water and EtOH, then cleaned with (b) THF via Soxhlet extraction, then washed with (c) Acetone via Soxhlet extraction; and TpBD.

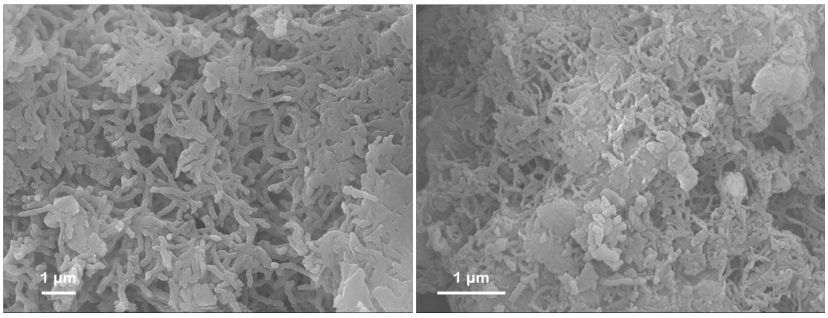

Figure S28 SEM images of TpBD

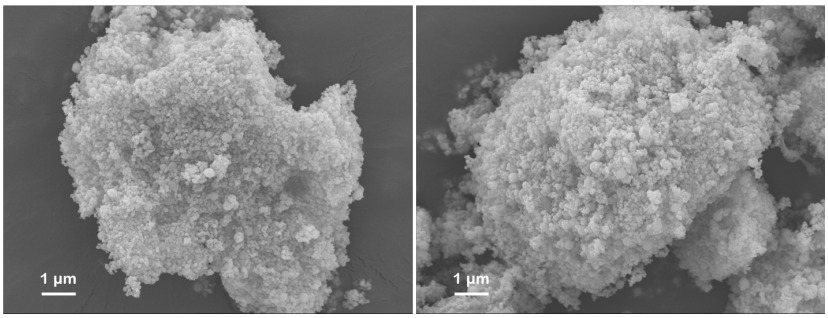

Figure S29 SEM images of CdS/TpBD-20%

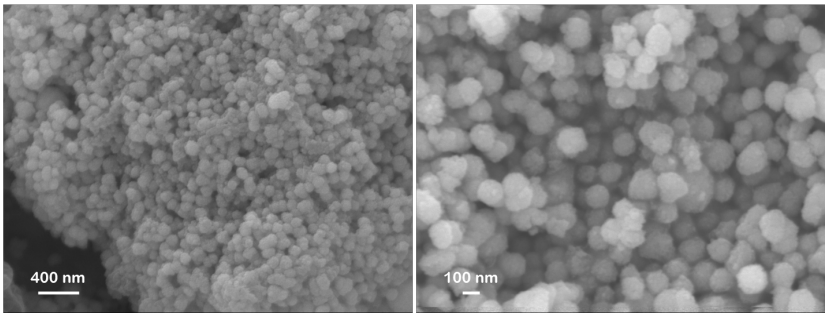

Figure S30 SEM images of CdS/TpBpy-20%/Co

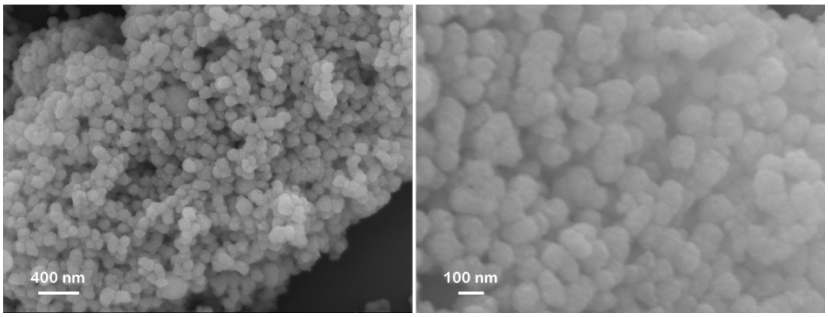

Figure S31 SEM images of used CdS/TpBpy-20%/Co

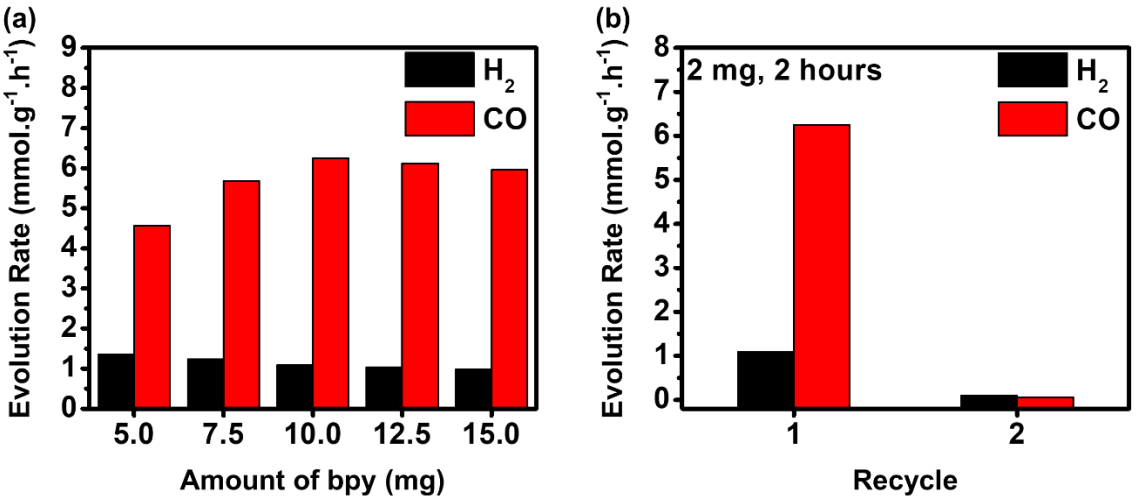

Figure S32 (a) Influence of bpy amount on the photocatalytic CO_2 reduction performance. Reaction condition: 2.00 mg of CdS/TpBpy-20%/Co, 5.0 ml of TEOA, 7.0 ml of MeCN, and 3.0 ml of water. (b) Catalyst recycling experiments of 2.00 mg of CdS/TpBpy-20%/Co. After 2-hour illumination, the used catalyst was collected by centrifugation, washed with MeCN (4x7 ml), and dried under reduced pressure at room temperature. Please note that the reactions using CdS/TpBpy-20%/Co were conducted without adding Co^{2+} ($CoCl_2$).

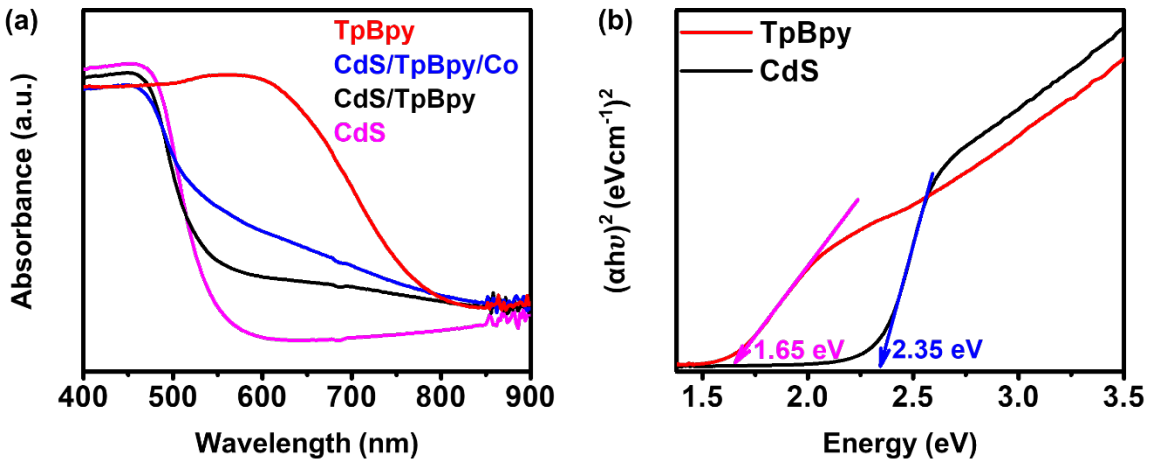

Figure S33 (a) UV-Vis diffuse reflectance spectra of the as-prepared materials. (b) Tauc plots of CdS and TpBpy.

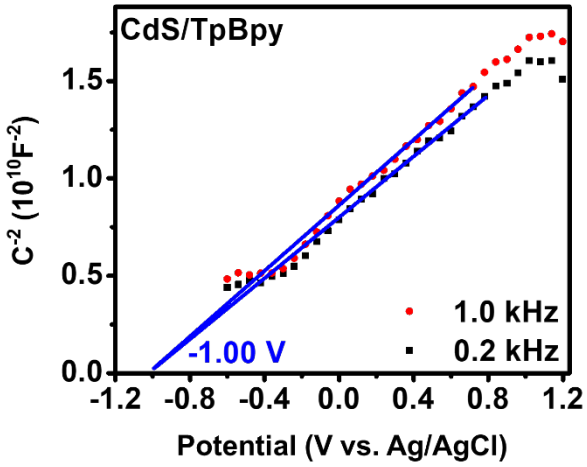

Figure S34 Mott-Schottky plots of CdS/TpBpy.

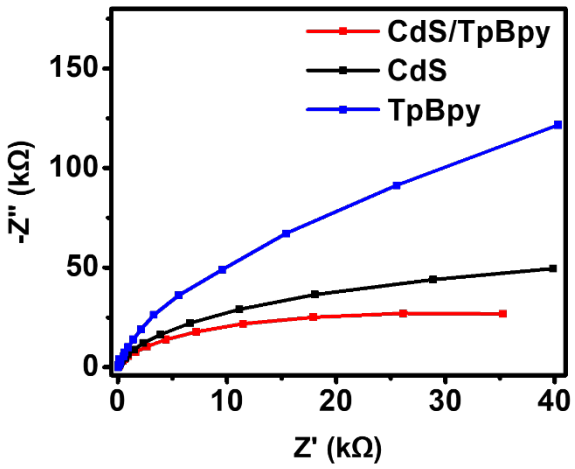

Figure S35 Impedance measurements of the as-prepared materials.

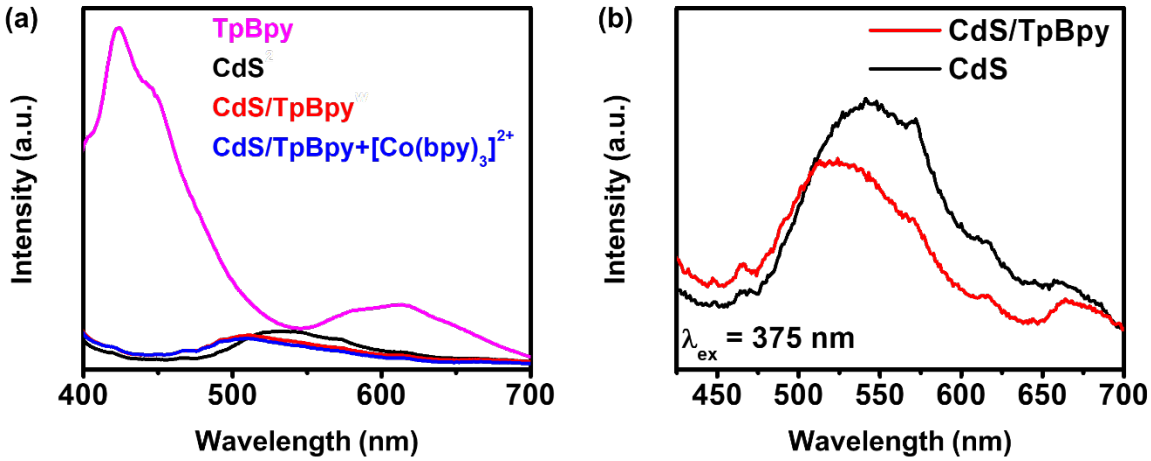

Figure S36 (a) PL spectra of the as-synthesized materials in EtOH. (b) Solid-state PL spectra of CdS and CdS/TpBpy.

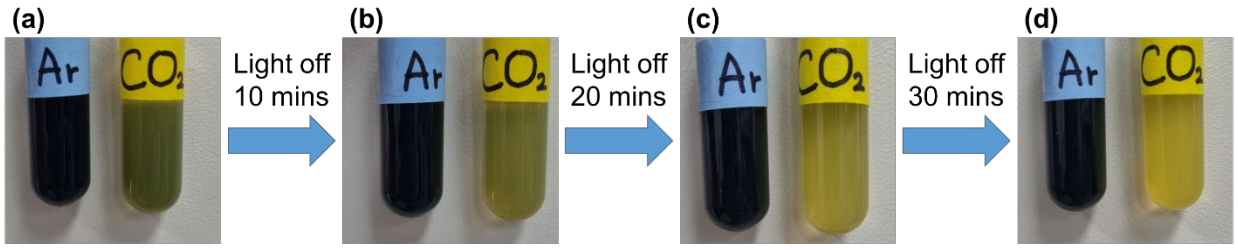

Figure S37 Photographs: (a) the reaction mixtures under Ar and CO_2 right after illumination, (b) after stopping reaction for 10 minutes, (c) after stopping reaction for 20 minutes, and (d) after stopping reaction for 30 minutes.

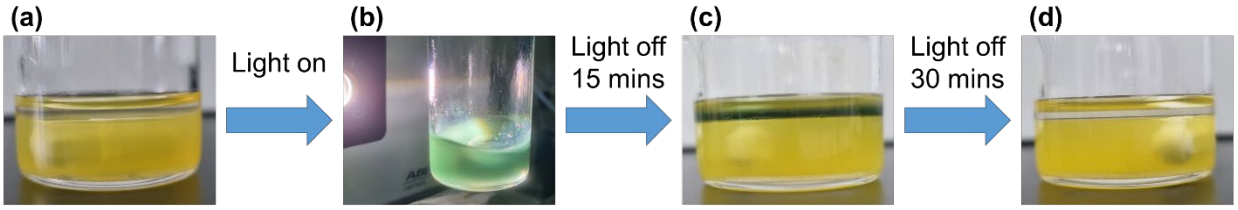

Figure S38 Photographs: (a) the fresh reaction mixture of CdS/TpBpy, (b) upon visible light irradiation, (c) after stopping reaction for 15 minutes, and (d) after stopping reaction for 30 minutes. The reaction medium was divided into two phases. The upper phase (organic phase) had the higher concentration of $[Co(bpy)_x]^+$ (Co^I species) [1, 2].

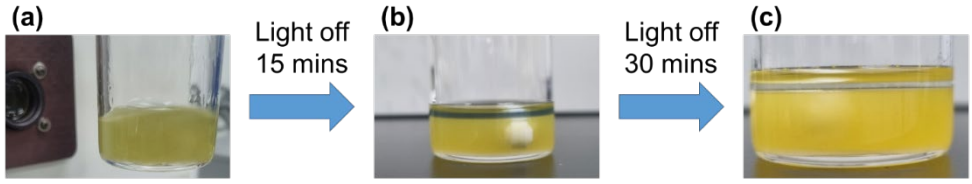

Figure S39 Photographs: (a) the reaction mixture of CdS/TpBpy-20%/Co right after illumination, (b) after stopping reaction for 15 minutes, and (c) after stopping reaction for 30 minutes. Please note that the reaction was conducted without adding Co^{2+} ($CoCl_2$). However, the reaction medium showed a blue layer after stopping illumination, indicating $[Co(bpy)_x]^+$ is extracted from CdS/TpBpy-20%/Co

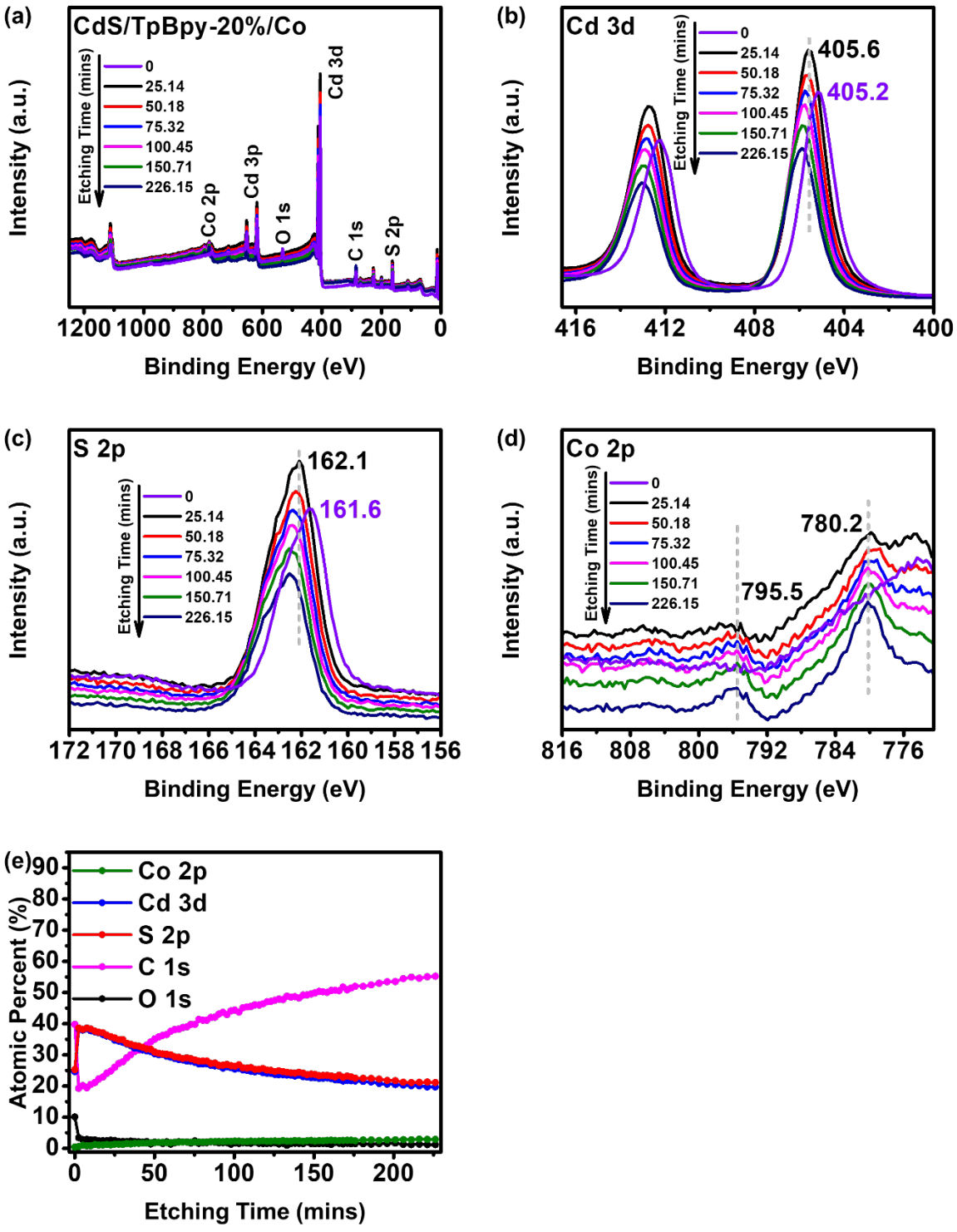

Figure S40 (a) XPS survey spectrum of CdS/TpBpy-20%/Co. (b) Cd 3d, (c) S 2p, and (d) Co 2p high resolution XPS spectra of CdS/TpBpy-20%/Co. (d) XPS atomic percentage of CdS/TpBpy-20%/Co.

Table S1 Cd and Co loadings of different samples analyzed by ICP-OES.

Sample	Cd loading (wt %)	Co loading (wt %)	CdS/(CdS+COF) (%)
CdS/TpBpy-10%	69.935		89.9
CdS/TpBpy-20%	61.174		78.6
CdS/TpBpy-30%	52.984		68.1
CdS/TpBpy-40%	43.949		56.5
CdS/TpBD-20%	59.483		76.4
CdS/TpBpy-20%/Co	55.570	3.10	76.6

Table S2 The fitting parameters of TRPL decay curves of CdS, CdS/TpBpy-20%, and CdS/TpBpy-20% + $[Co(bpy)_3]^{2+}$.

	τ_1 (ns)	A_1 (%)	B_1 (%)	τ_2 (ns)	A_2 (%)	B_2 (%)	τ (ns)	χ^2
CdS	0.0531	99.833	87.008	4.740	0.167	12.992	0.662	1.06
CdS/TpBpy-20%	0.2957	98.766	86.404	3.724	1.234	13.596	0.762	1.11
CdS/TpBpy-20% + $[Co(bpy)_3]^{2+}$	0.4539	93.482	69.167	2.902	6.518	30.833	1.209	1.15

The average lifetimes were calculated by the following equation:

$$\tau = \frac{A_1{\tau_1}^2 + A_2{\tau_2}^2}{A_1\tau_1 + A_2\tau_2}$$

where A_1 and A_2 represent the percentages of pre-exponential factors, while τ_1 and τ_2 denote decay times.

The fractional contributions of each decay component were calculated by the following equation:

$$B_1 = \frac{A_1\tau_1}{A_1\tau_1 + A_2\tau_2} \times 100$$

and

$$B_2 = \frac{A_2\tau_2}{A_1\tau_1 + A_2\tau_2} \times 100.$$

Table S3 Comparison of CO_2 photoreduction performance of different photocatalysts.

Catalyst	Solvent/Hole Scavenger/ Cocatalyst	Light Source	Major Product Evolution Rate ($\mu mol\ g^{-1}\ h^{-1}$)	Ref.
CdS/TpBpy	MeCN, water/TEOA/ $[Co(bpy)_3]^{2+}$	150 W Xe lamp Solar light	CO: 8800 AQE: 4.75 %	This work
ZnS-ETA/CdS	MeCN, water/TEOA/ $[Co(bpy)_3]^{2+}$	300 W Xe lamp ($\lambda \geq 420$ nm)	CO: 8325	[3]
Co_3O_4@$CdIn_2S_4$	MeCN, water/TEOA/ $[Co(bpy)_3]^{2+}$	300 W Xe lamp ($\lambda \geq 400$ nm)	CO: 5300 AQE: 1.87 %	[4]
3DOM CdSQD/NC	MeCN, water/TEOA/ $[Co(bpy)_3]^{2+}$	300 W Xe lamp ($\lambda \geq 420$ nm)	CO: 5210 AQE: 2.9 %	[5]
Au(25)@CdS	MeCN, water/TEOA/ $[Co(bpy)_3]^{2+}$	300 W Xe lamp ($\lambda \geq 400$ nm)	CO: 3758 AQE: 0.61 %	[6]
$ZnIn_2S_4$-CdS	MeCN, water/TEOA/ $[Co(bpy)_3]^{2+}$	300 W Xe lamp ($\lambda \geq 400$ nm)	CO: 3340	[7]
$ZnIn_2S_4$-In_2O_3	MeCN, water/TEOA; $[Co(bpy)_3]^{2+}$	300 W Xe lamp ($\lambda \geq 400$ nm)	CO: 3075	[8]
Co-ZIF-9/CdS	MeCN, water/TEOA; bpy	300 W Xe lamp ($\lambda \geq 420$ nm)	CO: 2520 AQE: 1.93 %	[9]
Ni-TpBpy $[Ru(bpy)_3]Cl_2$	MeCN, water/TEOA; bpy	300 W Xe lamp ($\lambda \geq 420$ nm)	CO: 966 AQE: 0.3 %	[10]
CdS/ZIF-8	MeCN, water/TEOA/ $[Co(bpy)_3]^{2+}$	300 W Xe lamp ($\lambda \geq 420$ nm)	CO: 803.3	[11]
CdS/BCN	MeCN, water/TEOA/ $[Co(bpy)_3]^{2+}$	300 W Xe lamp ($\lambda \geq 420$ nm)	CO: 250	[12]
CdS/UiO-bpy/Co	MeCN/TEOA	300 W Xe lamp ($\lambda \geq 420$ nm)	CO: 235 AQE: 0.65 %	[13]

References

1. J. L. Lin, R. Y. Liao and J. L. Xu, *RSC Adv.*, 2018, **8**, 3798-3802.
2. Q. Q. Mu, Y. H. Su, Z. H. Wei, H. Sun, Y. B. Lian, Y. Y. Dong, P. W. Qi, Z. Deng and Y. Peng, *J. Catal.*, 2021, **397**, 128-136.
3. B. Su, L. J. Huang, Z. Xiong, Y. C. Yang, Y. D. Hou, Z. X. Ding and S. B. Wang, *J. Mater. Chem. A*, 2019, **7**, 26877-26883.
4. L. J. Huang, B. F. Li, B. Su, Z. Xiong, C. J. Zhang, Y. D. Hou, Z. X. Ding and S. B. Wang, *J. Mater. Chem. A*, 2020, **8**, 7177-7183.
5. F. Wang, T. Hou, X. Zhao, W. Yao, R. Fang, K. Shen and Y. Li, *Adv. Mater.*, 2021, **33**, e2102690.
6. P. Zhang, S. B. Wang, B. Y. Guan and X. W. Lou, *Energy Environ. Sci.*, 2019, **12**, 164-168.
7. Z. Z. Zhu, X. X. Li, Y. T. Qu, F. Y. Zhou, Z. Y. Wang, W. Y. Wang, C. M. Zhao, H. J. Wang, L. Q. Li, Y. G. Yao, Q. Zhang and Y. Wu, *Nano Res.*, 2021, **14**, 81-90.
8. S. B. Wang, B. Y. Guan and X. W. D. Lou, *J. Am. Chem. Soc.*, 2018, **140**, 5037-5040.
9. S. B. Wang and X. C. Wang, *Appl. Catal., B Environ.*, 2015, **162**, 494-500.
10. W. Zhong, R. Sa, L. Li, Y. He, L. Li, J. Bi, Z. Zhuang, Y. Yu and Z. Zou, *J. Am. Chem. Soc.*, 2019, **141**, 7615-7621.
11. Y. Liu, L. Deng, J. P. Sheng, F. Y. Tang, K. Zeng, L. Q. Wang, K. X. Liang, H. Hu and Y. N. Liu, *Appl. Surf. Sci.*, 2019, **498**, 143899.
12. M. Zhou, S. B. Wang, P. J. Yang, C. J. Huang and X. C. Wang, *ACS Catal.*, 2018, **8**, 4928-4936.
13. C. J. Chen, T. B. Wu, H. H. Wu, H. Z. Liu, Q. L. Qian, Z. M. Liu, G. Y. Yang and B. X. Han, *Chem. Sci.*, 2018, **9**, 8890-8894.